Ultramicroscopy 111 (2011) 628–632

Contents lists available at ScienceDirect

Ultramicroscopy

journal homepage: www.elsevier.com/locate/ultramic

Atom probe tomography characterization of heavily cold drawn pearlitic steel wire

Y.J. Li [a,b,*], P. Choi [b], C. Borchers [a], Y.Z. Chen [a], S. Goto [c], D. Raabe [b], R. Kirchheim [a,b]

[a] Institut für Materialphysik, Georg-August-Universität Göttingen, Friedrich-Hund-Platz 1, D-37077 Göttingen, Germany
[b] Max-Planck Institut für Eisenforschung, Max-Planck-Str. 1, D-40237 Düsseldorf, Germany
[c] Department of Materials Science and Engineering, Faculty of Engineering and Resource Science, Akita University, Tegata Gakuencho, Akita 010-0852, Japan

ARTICLE INFO

Available online 24 November 2010

Keywords:
Atom probe tomography
Pearlitic steel wire
Cementite decomposition
Severe plastic deformation
Dislocations
Cell boundaries

ABSTRACT

Atom Probe Tomography (APT) was used to analyze the carbon distribution in a heavily cold drawn pearlitic steel wire with a true strain of 6.02. The carbon concentrations in cementite and ferrite were separately measured by a sub-volume method and compared with the literature data. It is found that the carbon concentration in ferrite saturates with strain. The carbon concentration in cementite decreases with the lamellar thickness, while the carbon atoms segregate at dislocations or cell/grain boundaries in ferrite. The mechanism of cementite decomposition is discussed in terms of the evolution of dislocation structure during severe plastic deformation.

1. Introduction

It is well known that severe plastic deformation, e.g. heavy cold drawing, can strengthen pearlitic steel wires. Depending on the drawing strain the interlamellar spacing can be refined to 5–20 nm [1–3] and the ultimate tensile strength reaches values between 3.2 and 5.0 GPa [1,4–8]. In addition, many efforts have been made to further enhance the wire strength by increasing the carbon content and/or adding Cr to the material [9–12]. In such cases, the tensile strength can be as high as 5.7 GPa for wires with a diameter of 40 μm [9]. The addition of Cr not only improves the strength of as-patented wires by refining their lamellar structure, but also increases the work hardening rates during cold drawing. The latter effect can also be obtained by increasing the carbon content [11]. Accompanied by the formation of a nano-scaled lamellar structure and the enhancement of wire strength, cementite is found to be partially amorphized [3,8,13] and to decompose upon plastic deformation. This makes an understanding of the strengthening mechanisms more complicated. The decomposition of cementite has been extensively investigated by means of Mössbauer spectroscopy [14], one-dimensional atom probe (1DAP) [4,6,11,13,15–17], and atom probe tomography (APT) [3,8,15,18–20]. Up to now, the mechanisms of cementite decomposition and the positions of carbon atoms in ferrite still remain unclear [19,21–24].

To better understand the mechanism of cementite decomposition, it is important to accurately quantify the carbon distribution in the material. The reliability of the quantification depends on the accuracy of the analytical tool as well as on the specimen preparation technique. For example, 1DAP has been frequently used to analyze the cementite decomposition. However, 1DAP is limited with respect to the analyzed volume and field of view [25]. Regarding the limitation of specimen preparation methods, the needle-shaped specimens for atom probe measurements were previously prepared by the conventional electro-polishing, before focused ion-beam (FIB) milling came into use [26–28]. In the case of pearlitic steel wire with a lamellar structure, the electro-polishing method restricts the accuracy of quantification because the specimen tips are parallel to the pearlitic lamellae. Thus, only very few (one or two) cementite lamellae can be detected and the spatial resolution in the direction perpendicular to the lamellar interfaces is very low, as pointed out by Takahashi et al. [29].

In the present work, we study the cementite decomposition of a heavily cold drawn (true strain $\varepsilon = 6.02$) Cr-containing pearlitic steel wire using a Local Electrode Atom Probe (LEAP), which enables analyses of cementite decomposition with a large field of view and high mass resolution. The tip-shaped specimens for LEAP measurements are prepared by the FIB based lift-out method with tips perpendicular to the lamellar interfaces, as demonstrated in [29]. This method increases the number of detected cementite lamellae and also enables analyses with a high depth resolution. The influence of the true wire strain on the cementite decomposition is analyzed by comparing our results with literature data for similar materials taken at different wire strains [6]. The mechanism of cementite decomposition and the possible positions of carbon atoms in ferrite are discussed.

* Corresponding author at: Max-Planck Institut für Eisenforschung, Max-Planck-Str. 1, D-40237 Düsseldorf, Germany.
Tel.: +49 211 6792853; fax: +49 211 6792333.
E-mail address: y.li@mpie.de (Y.J. Li).

0304-3991/$ - see front matter © 2010 Elsevier B.V. All rights reserved.
doi:10.1016/j.ultramic.2010.11.010

2. Experiments

2.1. Material

The material used in this work is a commercial pearlitic steel wire with hypereutectoid composition (Fe–0.98C–0.31Mn–0.20Si–0.20Cr–0.01Cu–0.006P–0.007S wt% or Fe–4.40C–0.30Mn–0.39Si–0.21Cr–0.003Cu–0.01P–0.01S at.%) provided by Suzuki Metal Industry Co., LTD. The wire with an initial diameter of 0.18 mm was patented. This process includes austenitization at 1223 K for 80 s followed by pearlitic transformation in a lead bath at 853 K for 20 s. The patented wire was then deformed by lubricated drawing to a final diameter of 8.85 μm corresponding to a true wire strain of $\varepsilon = \ln(d_0^2/d^2) = 6.02$, where d_0 and d are the initial and final diameters of the wire, respectively.

2.2. Local electrode atom probe and measurement conditions

A LEAP 3000X HR™, Cameca Instruments was employed to analyze the carbon distribution in three-dimensions. This equipment enables the analysis of volumes up to $100 \times 100 \times 1000$ nm^3 and a high detection sensitivity due to an improved mass resolution ($\Delta m/m =$ 1/1100, FWHM at 27 Da).

LEAP measurements were performed in voltage mode at 70 K under an ultra-high vacuum of 6×10^{-11} Torr. The total voltage during probing was in the range of 6.2–7.2 kV. The pulse fraction was 15%. The pulse repetition rate was 200 kHz at detection rate of 0.005 atom per pulse.

Samples for APT analyses were prepared with the tips perpendicular to the wire axis using a dual beam focused ion-beam (FIB) (FEI Helios NanoLab 600TM) according to the procedure described in [29].

3. Results

3.1. Mass spectrum analyses

The peaks in the mass spectrum at mass to charge ratios (m/n) 6, 6.5, 12, 13, 18, 18.5, 24, 24.5 and 36 Da are all due to carbon (m: ionic mass; n: ionization state). Since carbon atoms evaporate as both single ions (C^+ and C^{2+}) and molecular ions (C_2^+, C_2^{2+}, C_3^+ C_3^{2+} and C_4^{2+}), the peaks at $m/n = 12$ and 24 Da are ambiguous. While the peak at 12 Da can be assigned as either $^{12}C^+$ or $^{12}C_2^{2+}$, or a mixture of both, the ambiguity for the peak at 24 Da lies between $^{12}C_2^+$ and $^{12}C_4^{2+}$. A peak decomposition algorithm (supplied by the software IVAS, Cameca Instruments), which is similar to the method used by Sha et al. [30] and takes into account the isotope ratios, was applied to these two peaks. The results show that both signals can be ascribed to a mixture of ions. For the peak at 12 Da the contributions to this peak are 81% from $^{12}C^+$ and 19% from $^{12}C_2^{2+}$. Therefore, this peak is assigned as $^{12}C^+$ for the present measurement. For the peak at 24 Da the percentages are 48% from $^{12}C_2^+$ and 52% from $^{12}C_4^{2+}$, as shown in Table 1. Compared to the nominal carbon concentration (see Table 2), the assignments for this peak as $^{12}C_2^+$ or $^{12}C_4^{2+}$ lead to an underestimation of the carbon concentration by 16% or an overestimation by 4%, respectively. Taking the weight factors of the contributions from $^{12}C_2^+$ and $^{12}C_4^{2+}$ to the peak into account, the calculated overall carbon concentration is 4.4 at.%, which virtually equals the nominal one. This means that the LEAP has accurately detected the carbon element in pearlitic steel wires. For the 3D elemental map, the assignment of this peak to $^{12}C_4^{2+}$ is reasonable.

Note that the assignment of the peak at 24 Da may differ between cementite and ferrite if their mass spectra are analyzed separately. Indeed, as described in Section 3.2.2, the contributions to this peak are 100% from C_2^+ in ferrite, while 85–90% from C_4^{2+} in cementite.

Table 1
Results from peak decomposition performed for the peak at 24 Da.

Ion type	% of range	Decomposition abundance
$^{12}C_2^+$	48	0.98
$^{12}C_4^{2+}$	52	0.95

3.2. Carbon concentration in cementite and ferrite

3.2.1. 1D carbon concentration profiles

Fig. 1(a) shows the 3D atom map for carbon. To visualize the morphology and size of the cementite lamella, a carbon isoconcentration surface drawn at 7 at% is shown. Due to a relatively sharp carbon concentration profile at the interface-near region, the selection of iso-value is not critical for the present case. The iso-value of 7 at.% C is selected using the criterion that a phase with a carbon concentration above 7 at.% cannot be ferrite and is therefore defined as cementite. With this definition the morphology and size of the cementite lamella are visualized.

Table 2
Comparison between chemical compositions measured by LEAP, using two different assignments of the peak at 24 Da, and the nominal values. Unit: at.%.

Element	Nominal	LEAP $^{12}C_2^+$	LEAP $^{12}C_4^{2+}$
Fe	94.670	94.409	93.565
C	**4.410**	**3.708**	**4.569**
Si	0.390	0.447	0.443
Cr	0.210	0.214	0.212
Mn	0.300	0.284	0.281
Cu	0.009	0.003	0.003
P	0.010	0.005	0.005
S	0.010	0.008	0.008
Ga	–	0.921	0.913

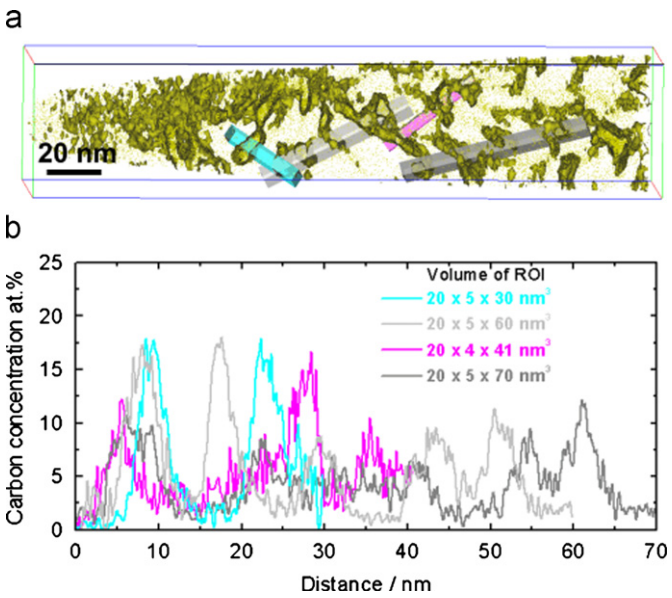

Fig. 1. (a) 3D carbon atom map (containing over 12×10^6 ions within a volume of $55 \times 55 \times 230$ nm^3) with selected boxes for the regions of interest (ROIs). The carbon isoconcentration surface was drawn at 7 at.%. (b) 1D carbon concentration profiles (fixed bin width of 0.2 nm) for the selected boxes along the main axes of ROIs. The ROIs and the corresponding concentration profiles are related to each other by the same colors.

Frequently, cementite decomposition has been quantitatively analyzed by plotting an 1D carbon concentration profile for a selected box containing many lamellae [15,29]. In Fig. 1(a) four regions of interest (ROIs) of different colors are selected for analysis. The advantage of this method is that the extent of both the cementite decomposition and the amount of carbon in the ferrite can be immediately taken from the concentration profiles. As shown in Fig. 1(b), the peak values of carbon concentration lie between 7 and 18 at.% for carbon-enriched lamellae and between 1 and 3 at.% for carbon-depleted regions.

However, this method can only provide a rough quantification of the carbon concentration. The reasons are as follows. First, since the surface atoms evaporate layer by layer during probing and each layer contains two different phases with different evaporation fields, the so-called local magnification effect appears. In the case of pearlite cementite is known to have a lower evaporation field than ferrite [20,31]. This leads to a widened apparent carbon concentration gradient at the interfaces between ferrite and cementite. Thus, the carbon concentration from 1D concentration profiles strongly depends on the dimensions of the analysis box selected. If we take a look at the spatial orientations and the morphologies of cementite lamellae from the 3D atom map shown in Fig. 1(a), the cementite lamellae have decomposed and/or fragmented into various forms with various sizes regarding the cross-sections of the cementite lamellae. Therefore, the local magnification effect cannot be avoided. Secondly, since the assignment of the peak at 24 Da differs between cementite and ferrite, as will be further analyzed in Section 3.2.2, a ROI including both cementite and ferrite phases cannot give an accurate quantification of the carbon concentration in each phase. If the peak at 24 Da is assigned to $^{12}C_4^{2+}$ for such a ROI, the carbon concentration in ferrite is overestimated. Otherwise, the carbon concentration in cementite will be underestimated.

3.2.2. *Quantification of carbon concentration by the sub-volume method*

In the following, the sub-volume method is used to treat different phases separately and thus obtaining higher compositional accuracy.

Fig. 2 displays the analysis procedures of the sub-volume method. For cementite, the ROIs (green) are selected and positioned individually for each lamella in such a way that they contain the largest possible volume without any matrix included. Here, the matrix is defined as a phase with carbon concentration lower than 7 at.%. For ferrite, the ROIs (pink) are selected from the matrix, which is, however, defined as a phase with carbon concentration lower than 3 at.%. This is to make sure that the selected ROIs for ferrite are kept far away from the interface-near zones, where the local magnification effect is significant. All the selected ROIs are cut away from the whole volume and their mass spectra are analyzed separately. Peak decomposition is performed for the peak at 24 Da for each selected sub-volume. Figs. 2(b) and (d) show ROIs representing cementite and ferrite, respectively. The results from peak decomposition show that 100% of the range for the peak at 24 Da is due to $^{12}C_2^+$ for ferrite, while 86% is due to $^{12}C_4^{2+}$ for cementite. Based on these assignments, the average carbon concentration in ferrite is determined to be 0.60 at.% for the ROI. For cementite, the maximum carbon concentration, i.e. the concentration measured in the middle of the cementite lamella is 17.5 at.% (see Fig. 2c) and this value is taken as the composition of the selected ROI.

Fig. 3 shows the average carbon concentrations in ferrite for all the ROIs as a function of wire strain. The data for wire strains $\varepsilon < 5$ from [6] are also shown for comparison. It is seen that the obtained values are different even for the same strain. Since no detail for the determination of carbon concentrations in [6] is given, it is hard to explain the large scatter of the values for the same strain. Due to the local magnification effect, the carbon concentration in ferrite strongly depends on the location of the selected ROI. For the data at $\varepsilon = 6.02$, obtained from the present work, such an influence can be mostly eliminated. Therefore, the variation of the concentrations indicates that the distribution of the carbon atoms is inhomogeneous in ferrite.

To clarify the dependence of carbon concentration on the wire strain, the final average values for each strain are plotted as the red

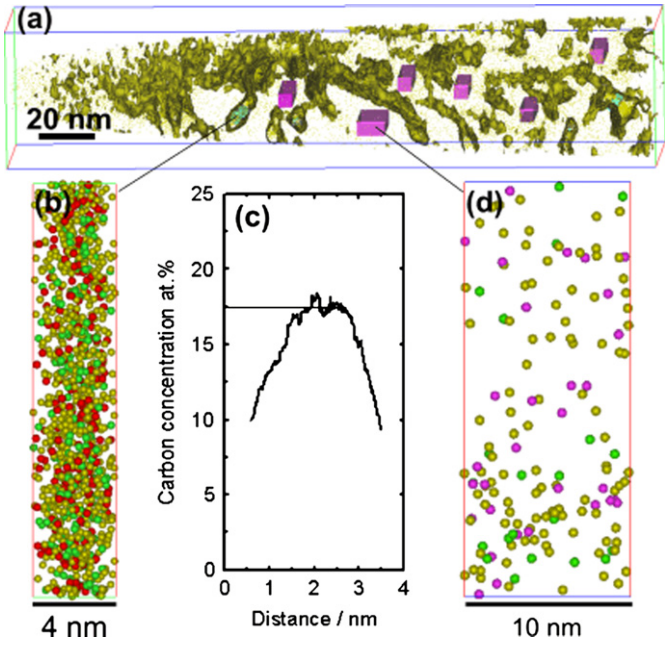

Fig. 2. Example showing the analysis procedures of sub-volume method. (a) The whole reconstructured 3D image with the selected sub-volumes to be cut. Green for cementite and pink for ferrite. (b) Atom map for a selected sub-volume of cementite cut from (a). The different color spheres represent different species of carbon. Yellow for C^+ and C^{2+}, pink for C_2^+, green for C_3^{2+} and red for C_4^{2+}. (c) 1D carbon concentration profile for the ROI of (b). As shown by the thin horizontal line, the value at the center of the profile is taken for the lamella. (d) As (b) for ferrite. (For interpretation of the references to color in this figure legend, the reader is referred to the web version of this article.)

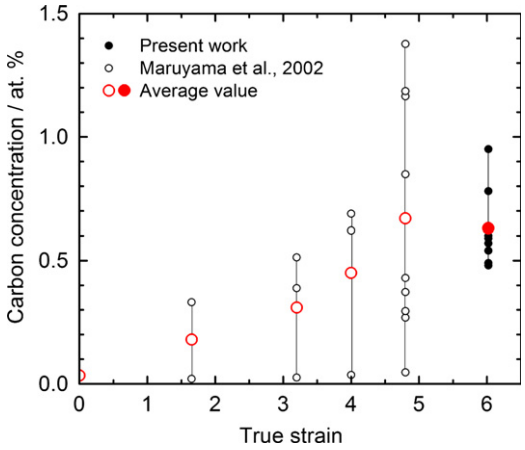

Fig. 3. Carbon concentrations in ferrite as a function of wire strain for hypereutectoid pearlitic steel wires. Literature data (Cr free) from [6] are displayed as small black open circles. The large red symbols represent the final average values calculated from all the data shown for each strain. (For interpretation of the references to color in this figure legend, the reader is referred to the web version of this article.)

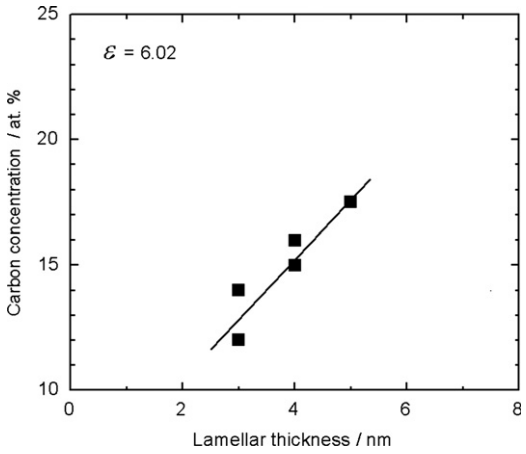

Fig. 4. Carbon concentrations in the cementite as a function of lamellar thickness.

circles shown in Fig. 3. For $\varepsilon < 5$, the carbon concentration increases with increasing wire strain. This implies that plastic deformation promotes the cementite decomposition up to $\varepsilon \approx 5$. For $\varepsilon > 5$, the carbon concentration in the ferrite appears to reach the saturated state. The slightly higher value measured at $\varepsilon = 4.7$ from [6] than that for $\varepsilon = 6.02$ may result from the local magnification effect, which will get more pronounced, if the probing direction is parallel to the lamellar interfaces. This is exactly the case in [6]. It may also result from the differences between the materials used in [6] and the present work. It is known that Cr has the effect of strengthening the bonds of the cementite lattice [32], and thus suppresses cementite decomposition. In addition, the data evaluation method is also crucial to the obtained concentration values, as stated in Section 3.2.1. No detail on the analysis of the quantification is given in [6].

Fig. 4 displays the carbon concentrations measured in the middle of the analyzed cementite lamellae as a function of lamellar thickness. The use of concentration values at the center of the lamella may be a pertinent approach to quantify the extent of cementite decomposition, since they remain unaffected by the local magnification effect. For each cementite lamella, its thickness is determined based on the isoconcentration surfaces drawn at 7 at.% C. The results show that no cementite with a stoichiometric carbon concentration remains after heavy cold drawing. Also, we observe that thinner lamellae are more prone to undergo deformation-induced chemical decomposition than thicker lamellae. This observation was not reported before in the literature.

4. Discussion

Although it is well accepted that cementite decomposes during cold deformation of pearlitic steel, the predominant decomposition mechanism is still under discussion. Mainly two interpretations are used to explain this phenomenon. One is based on thermodynamic considerations and the other one on carbon–dislocation interactions in ferrite. The first one attributes the decomposition to a reduction in thermodynamic stability of cementite caused by refinement of the lamellae structure and the increase of steps on their surfaces [23]. The second one suggests that the decomposition is driven by the difference between the high bonding energy between dislocations and carbon atoms in ferrite (0.75 eV [33]) and the low binding energy between the atoms of iron and carbon in cementite (0.40−0.42 eV [34,35]). Thus, dislocations drag carbon atoms out of cementite during deformation [21,22]. Based on the present APT results, we consider that the second approach might be the more likely mechanism of atomic-scale mixing across the hetero-interfaces. Beyond the elementary interaction between carbon atoms and lattice dislocations, which can carry the solutes into the ferrite and acts as pipe-diffusion channels, we also consider a dislocation-shuffle mechanism to contribute to the deformation-enhanced mixing process. Dislocation-shuffling refers to a phenomenon of trans-phase plastic dislocation slip (from ferrite into the cementite), potentially on more than one slip system. Such shearing of atomic planes through dislocation glide on more than one slip system across the interface of abutting layers can create small embedded particles consisting of atoms from one phase in the other. Such tiny material portions can be further cut by dislocations running through them, thereby increasing their energy through the Gibbs–Thomson effect so that they finally dissolve. In principle this mechanism can explain the large deformation-driven mass transport among the two phases against the thermodynamic equilibrium conditions. This and related possible mechanisms that may lead to deformation-induced chemical non-equilibrium mixing were recently discussed in [36].

According to the carbon–dislocation interaction mechanism, dislocations mainly get stored at the phase boundary between ferrite and cementite during severe plastic deformation. The ferrite matrix is relatively free of dislocations. This is reasonable if the mean free path of dislocations is larger than the interlamellar spacing. To make a safe estimate, let us assume a typical dislocation density of $\rho = 10^{16}/m^2$ in the material after a drawing strain of 6.02. The mean free path of dislocations may be estimated with a small prefactor 10 to be $10\rho^{-0.5} = 100$ nm, which is 10 times larger than the measured interlamellar spacing of 12 nm. Clearly, the motion of dislocations must be hindered by the phase boundaries. Indeed, in many TEM studies a large density of dislocations are observed at phase boundaries [23,37]. On the other hand, one should not totally rule out the possibility of formation of cell boundaries and/or grain boundaries inside ferrite lamellae during severe plastic deformation. In fact, Tarui et al. [11] observed cell structures in the size of 10 nm in the ferrite of a pearlitic steel wire with $\varepsilon = 4.2$ by TEM. The material used in the present work has been further strained by a strain of approximately 2, the cell structure is expected to evolve towards (sub)grain structures with few dislocations inside the cells/grains.

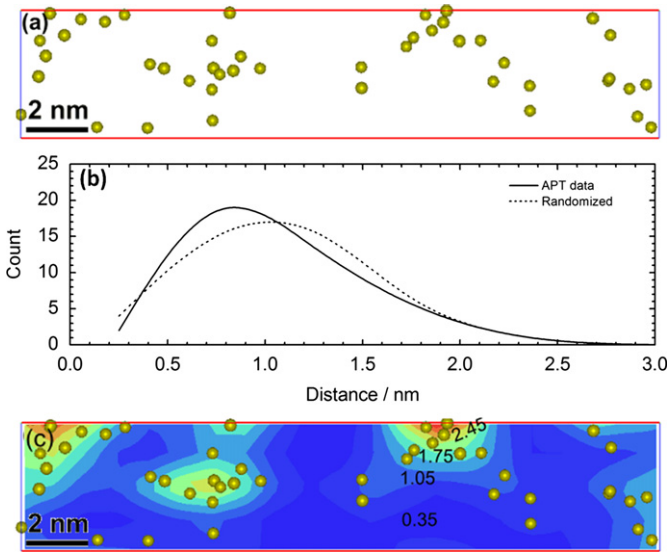

Fig. 5. (a) Carbon atom map for a selected ROI ($20 \times 3 \times 4\ nm^3$) from matrix showing inhomogeneous distribution of atoms in ferrite. (b) Distribution of the first nearest neighbor distance between carbon atoms in (a). Solid and dashed plots represent the observed data and the randomly reordered data, respectively. (c) Carbon contour plot with 0.3 nm distances between both samples and sampling planes. The numbers mark the local carbon concentrations in atomic percentage.

Fig. 5(a) shows an inhomogeneous distribution of carbon atoms in a selected volume in ferrite. The deviation of the calculated pair-distance distribution from the randomized one shown in Fig. 5(b) quantifies the inhomogeneity. The 2D concentration profile shown in Fig. 5(c) marks the local concentrations. It is likely that the areas with high carbon concentrations mark the cell/grain boundaries or individual dislocations, where the carbon concentration is five times higher than that in the interior. The atoms segregated at these boundaries may be directly carried here by dislocations leaving from the phase boundaries. They may also diffuse from the phase boundaries through dislocation cores.

An interesting observation is the decrease in carbon concentration in cementite with decreasing cementite thickness (Fig. 4). From this we can infer that a decrease of the cementite thickness in the as-patented material promotes cementite decomposition during deformation. This is understandable because for a given volume of total cementite, the thinner the cementite lamella, the higher the fraction of the phase boundary, and also the lower the interlamellar spacing. This would enhance the dislocation density at the phase boundaries upon deformation and therefore improve cementite decomposition. On the other hand, if the thin cementite lamellae are the remaining of a heavily dissolved originally coarse cementite, then the cementite must have undergone a strong local deformation which involves a large amount of dislocations. Thus, this would be a strong hint towards the importance of dislocations on cementite decomposition.

5. Conclusions

Cementite decomposition in a Cr-containing pearlitic steel wire caused by cold drawing up to a true strain of 6.02 was studied using atom probe tomography. It is found that the decomposition of cementite reduces their carbon concentration to 12–18 at.% and enhances the average carbon concentration in ferrite to 0.63 at.%. The comparison of the measured carbon concentrations in ferrite with literature data shows that plastic deformation promotes the cementite decomposition up to the wire strain of 5. For $\varepsilon > 5$ the decomposition process seems to reach its saturated stage. The carbon concentration in cementite varies proportionally with the thickness of the cementite lamella. These quantitative analyses together with the inhomogeneous distribution of carbon atoms in the ferrite allow us to conclude that the decomposition of cementite is presumably controlled by carbon–dislocation interactions, probably in conjunction with trans-phase dislocation shear effects (dislocation shuffling). We assume that the carbon atoms are preferentially segregated at cell/grain boundaries or individual dislocations in ferrite.

Acknowledgments

The authors thank Dr. H. Yarita from Suzuki Metal Industry Co., LTD. for providing the cold drawn specimens, and Dr. D. Ponge from Max-Planck Institut für Eisenforschung for valuable discussion. We also thank U. Tezins and A. Sturm for their help with LEAP measurements and FIB-based specimen preparation. We are grateful to the Deutsche Forschungsgemeinschaft for funding this research.

References

[1] A. Taniyama, T. Takayama, M. Arai, T. Hamada, Scr. Mater. 51 (2004) 53.
[2] G. Landford, Metall. Trans. A 8 (1977) 861.
[3] C. Borchers, T. Al-Kassab, S. Goto, R. Kirchheim, Mater. Sci. Eng. A 502 (2009) 131.
[4] H.G. Read, W.T. Reynolds Jr., K. Hono, T. Tarui, Scr. Mater. 37 (1997) 1221.
[5] H. Tashiro, Nippon Steel Tech. Rep. 80 (1999).
[6] N. Maruyama, T. Tarui, H. Tashiro, Scr. Mater. 46 (2002) 599.
[7] M. Zelin, Acta Mater. 50 (2002) 4431.
[8] S. Goto, R. Kirchheim, T. Al-Kassab, C. Borchers, Trans. Nonferrous Met. Soc. China 17 (2007) 1129.
[9] T. Takahashi, I. Ochiai, H. Tashiro, S. Ohashi, S. Nishida, T. Tarui, Nippon Steel Tech. Rep. 64 (1995) 45.
[10] H. Tashiro, S. Nishida, T. Tarui, S. Ohashi, S. Sasaki, K. Nakamura, A. Yoshie, H. Demachi, Nippon Steel Tech. Rep. 80 (1999) 38.
[11] T. Tarui, N. Maruyama, J. Takahashi, S. Nishida, H. Tashiro, Nippon Steel Tech. Rep. 91 (2005) 56.
[12] T. Ochi, S. Nishida, M. Sugiyama, J. Takahashi, T. Tarui, Nippon Steel Tech. Rep. 96 (2007) 5.
[13] M.H. Hong, W.T. Reynolds Jr., T. Tarui, K. Hono, Metall. Mater. Trans. A 30 (1999) 717.
[14] V.N. Gridnev, V.G. Gavrilyuk, Y.D. Ekhtyayru, Y.A.M. Eshkov, P.S. Nizina, V.G. Prokopenko, Phys. Status Solidi A 11 (1972) 689.
[15] K. Hono, M. Ohnuma, M. Murayama, S. Nishida, A. Yoshie, Scr. Mater. 44 (2001) 977.
[16] T. Tarui, T. Takahashi, S. Ohashi, R. Uemori, Ironmaking Steelmaking 21 (1994) 25.
[17] T. Tarui, T. Takahashi, H. Tashiro, S. Nishida, in: H.G. Paris, D.K. Kim (Eds.), Processing and Applications of Metal Wires, TMS, Warrendale, PA, 1996, p. 87.
[18] F. Danoix, D. Julien, X. Sauvage, J. Copreaux, Mater. Sci. Eng. A 250 (1998) 88.
[19] X. Sauvage, J. Copreaux, F. Danoix, D. Blavette, Philos. Mag. A 80 (2000) 781.
[20] X. Sauvage, W. Lefebvre, C. Genevois, S.OhsakiK. Hono, Scr. Mater. 60 (2009) 1056.
[21] V.G. Gavriljuk, Scr. Mater. 45 (2001) 1469.
[22] V.N. Gridnev, V.V. Nemoshkalenko, Y.Y. Meshkov, V.G. Gavrilyuk, G. Prokopenko, O.N. Razumov, Phys. Status Solidi A 31 (1975) 201.
[23] J. Languillaume, G. Kapelski, B. Baudelet, Acta Mater. 45 (1997) 1201.
[24] X. Sauvage, Y. Ivanisenko, J. Mater Sci. 42 (2007) 1615.
[25] T.F. Kelly, M.K. Miller, Rev. Sci. Instrum. 78 (2007) 031101.
[26] M.K. Miller, K.F. Russell, G.B. Thompson, Ultramicroscopy 102 (2005) 287.
[27] M.K. Miller, K.F. Russell, K. Thompson, R. Alvis, D.J. Larson, Microsc. Microanal. 13 (2007) 428.
[28] K. Thompson, D. Lawrence, D.J. Larson, J.D. Olson, T.F. Kelly, B. Gorman, Ultramicroscopy 107 (2007) 131.
[29] J. Takahashi, T. Tarui, K. Kawakami, Ultramicroscopy 109 (2009) 193.
[30] W. Sha, L. Chang, G.D.W. Smith, L. Cheng, E.J. Mittemeijer, Surf. Sci. 266 (1992) 416.
[31] X. Sauvage, L. Thilly, D. Blavette, J. Phys. IV Fr. 11 (2001) 27.
[32] A. Inoue, T. Masumoto, Trans. ISIJ 17 (1977) 143.
[33] A.W. Cochardt, G. Schoek, H. Wiedersich, Acta Metall. 3 (1955) 533.
[34] R.A. Johnson, G.I. Diens, A.C. Damask, Acta Metall. 12 (1964) 125.
[35] R.A. Johnson, Acta Metall. 15 (1967) 513.
[36] D. Raabe, S. Ohsaki, K. Hono, Acta Mater. 57 (2009) 5254.
[37] M. Janecek, F. Louchet, B. Doisneau-Cottignies, Y. Brèchet, N. Guelton, Philos. Mag. A 80 (2000) 1605.